Oblique plies for steering through-thickness delamination migration in fibre reinforced polymers

Rafael Luterbacher[*], Richard S. Trask[†] and Ian P. Bond[‡]

University of Bristol, Bristol BS8 1TR, United Kingdom

The damage tolerance of safety critical aerospace structures is of paramount importance to ensure the airworthiness and safe operation of an aircraft. The ongoing transition from metallic to composite airframes requires a change in design philosophy to accommodate the fundamentally different behavior of composite structures in the event of damage, if future designs are not to be constrained or compromised, resulting in an inability to fully exploit the significant potential offered by composites. This work presents a feasibility study for an innovative method by which delaminations (a fundamental damage mechanism) can be steered through the thickness of a composite laminate. Plies with fibres oriented in the propagation direction are angled through the thickness in order to guide delamination migration. Static testing (Mode I) has shown the viability of this mechanism. In addition, a significant increase in fracture toughness, ranging from 88% to 269% depending on the configuration, is observed due to delamination branching and steering away from the

---

[*] PhD Student, Advanced Composites Centre for Innovation and Science (ACCIS), Queen's Building, AIAA member.

[†] Reader in Multifunctional Materials, Advanced Composites Centre for Innovation and Science (ACCIS), Queen's Building.

[‡] Professor and Head of the Department of Aerospace Engineering, Advanced Composites Centre for Innovation and Science (ACCIS),Queen's Building.

preferential propagation plane. Tensile and flexural testing has been performed in order to quantify the effect of this innovative architecture on the global mechanical properties. A significant knockdown in longitudinal tensile strength by up to 57% has been observed, while the effect on stiffness and flexural properties seems to be less significant. In addition the potential of applying the steering mechanism in skin-stiffener debond specimens under fatigue loading has been successfully demonstrated. Similar stiffness decay as for the baseline configuration is observed over 40000 cycles. The work in this study illustrates the potential for tailored fibre architectures, with a through-thickness feature, to provide a viable mechanism for steering critical damage into designated regions which are non-structural or contain added functionality to mitigate that damage

Nomenclature

Δa = Increment in delamination length, in m

b = specimen width, in m

E_f = Flexural modulus, in MPa

F = Load, in N

$F_{0.0005}$ = Load corresponding to a strain of 0.0005 in the four point bend test, in N

$F_{0.0025}$ = Load corresponding to a strain of 0.0025 in the four point bend test, in N

G_{Ic} = Strain energy release rate in Mode I, in J/m^2

h = specimen height, in mm

L = outer span in the four point bend test, in mm

s = mid-point deflection during 4 point bend test

$s_{0.0005}$ = Mid-point deflection corresponding to a strain of 0.0005 in the four point bend test, in mm

$s_{0.0025}$ = Mid-point deflection corresponding to a strain of 0.0025 in the four point bend test, in mm

W_{ext} = External work, in J

W_{strain} = Strain energy, in J

ϵ_f = strain at the outer surface in the four point bend test, in mm/mm

σ_f = flexural stress, in MPa

I. Introduction

The use of fibre reinforced polymers (FRP) has become increasingly prominent in the field of aeronautics currently accounting for approximately 50% of the structural weight of the Boeing 787 and Airbus A350. The major reason for the increased usage of FRP is the reduced maintenance due to the lack of corrosion and their high specific strength and stiffness[1]. However, even though the manufacturing and computational methods have advanced since the first use of composites in aeronautical applications, the design approach continues to exploit these materials as "black aluminium", where mainly quasi-isotropic lay-ups are used. Thus, the potential of FRPs are not yet being fully exploited. Unless required for local reinforcement, e.g. for areas experiencing higher loads or around stress concentrations, structures have a homogenous thickness with constant ply orientations in the different layers.

Damage tolerance within FRPs is another field of intense study[2–9] as the current design philosophy in aeronautical structures takes a "no damage growth" approach[10], leading to overdesign in the structure assuming the presence of damage from the outset. A large number of failure modes exist for FRPs in terms of the fibre and matrix constituents' e.g. intralaminar and interlaminar failure, where the latter generally leads to a progressive failure such as delamination growth. The research into increased damage tolerance for the polymer matrix has focused on the development of several approaches, including tougher resins, z-pinning or stitching, localised interleaving and improved structural design as discussed by *Greenhalgh et al*[11]. However, these approaches require complex or additional processing stages, additional materials or tend to compromise the overall laminate design.

Aircraft maintenance costs correspond to an important part of the life cycle costs of an aircraft [12]. Visual inspection is generally performed after each flight on an aircraft in order to detect any major damage event. However, in the case of FRP structures, a critical damage state can arise from barely visible damage[13], which can be caused by relatively modest impact damage. In this case, internal damage in terms of delaminations, matrix cracking and fibre fracture can be present, which significantly reduces the mechanical performance of the structure in the absence of any amelioration. Efforts are underway within the aerospace industry to develop methods by which such

barely visible damage manifests itself more clearly. For example, Boeing have patented a design[14] involving Poisson's ratio mismatch in order to redirect damage towards the outer surfaces and thereby arresting any cracks. This provides an additional benefit in that it makes internal damage more clearly visible.

An example of improved 'damage tolerant' structural design is a bio-inspired T-joint manufactured by *Burns et al.*[15]. In this case the T-joint mimics the structure of a tree branch to trunk joint. In contrast to conventional T-joints, where the web is secondary bonded or co-cured to the flange, the authors showed that by embedding a percentage of the plies from the web into the flange, the damage tolerance and the failure load of the T-joint was increased when compared to conventional T-joints.

Other examples from nature where the orientation of stiff laminar phases, comparable to the fibre direction of FRP plies, is used to control damage progression include the equine hoof wall[16] and the radula of snails[17]. In these cases the stiff laminar phases are oriented obliquely to the expected direction of damage propagation, redirecting the damage away from critical areas, such as soft tissue.

Delaminations are one of the critical failure modes of FRPs[18] and they are initiated by through-thickness stresses i.e. out of plane loading. *Singh et al.*[19] described two different mechanisms of delamination propagation: (1) propagation along the resin rich interlayer between plies, and (2) migration into other interfaces by ply splitting. *Purslow*[20] showed that delaminations tend to propagate along ply interfaces with plies oriented in the propagation direction. If these plies are oriented out of the plane, it should be possible to control the progression of the delamination. Steering of delaminations into preferential planes is beneficial for a variety of reasons. Moving a delamination to an outside surface is beneficial for damage visibility, rendering barely visible impact damage into visible damage thereby reducing inspection time and costs. In contrast, in terms of buckling resistance, it would be beneficial to steer a delamination into the mid-plane of a laminate in order to produce two sub-laminates with equal thickness and the same buckling strength. Also, steering of delaminations into predefined areas could be beneficial for both damage sensing and autonomous repair[21].

This work is composed of two different parts. The first is a feasibility study to demonstrate the ability of crack redirection using oblique plies (refer to Fig. 1) under Mode I loading, and their effect on global properties as

evidenced by tensile and flexural loading. The second is an investigation into introducing such a steering mechanism into a recognised skin-stiffener debond configuration[22,23] .

II. Feasibility study

A. Materials and lay up

Four different ply structures have been investigated; baseline (ID A), a very acute (4°) scarf angle (ID B), a less acute (15°) scarf angle (ID D) and a butted joint (ID E) (refer to Fig. 1). The very acute specimens were manufactured by staggering two plies every millimetre whereas the less acute configuration, one ply was staggered every two millimetres. The butted joint was studied as an extreme case.

In all cases with a scarf joint, the ply or plies removed from the central region were 0° plies. The selected lay-ups were $[-45_2/90_2/45_2/0_2]_S$ for the tensile and flexural specimens and $[0_4/-45_2/90_2/45_2/0_2]_S$ for the Mode I specimens. All panels were manufactured by hand lay-up. The material used was pre-impregnated unidirectional E-glass/913 epoxy resin (Hexcel), which was cured according to the manufacturer's recommended curing cycle (60 min at 125°C and 700 kN/mm^2, heat-up rate 2°C/min).

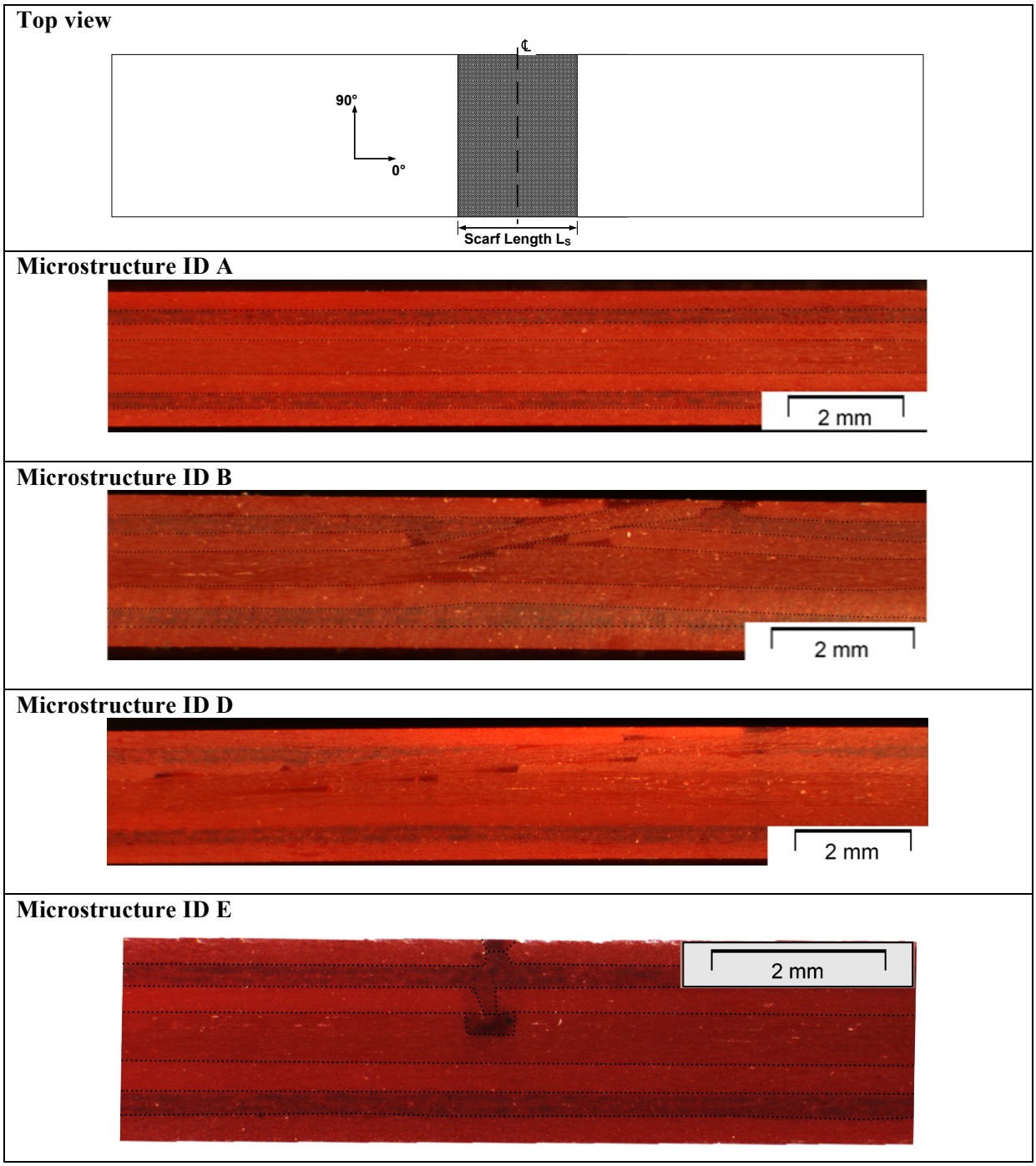

Fig. 1. Micrographs depicting ply structure within the specimens (for tensile and flexural testing). In the case of the DCB specimens, the exterior 0_4 plies are continuous.

B. Test Methods

1. *Mode I testing*

A Shimadzu AGS-X universal testing machine, equipped with a calibrated 1 kN load cell was used for double cantilever beam (DCB) testing. A LabVIEW™ script was used to acquire the delamination length, displacement and load data. Testing was performed in accordance with ASTM D5528[24]. Double Cantilever Beam (DCB) specimens were tested under displacement control at a rate of 5 mm/min. For data analysis the area method was selected[25]. Fracture toughness, G_{Ic}, is defined as follows:

$$G_{Ic} = \frac{\Delta W}{b \cdot \Delta a} = \frac{W_{ext} - W_{strain}}{b \cdot \Delta a} \quad (1)$$

Where b is the width of the specimen, Δa is the increment in delamination length, W_{ext} is the external work and W_{strain} is the strain energy. Refer to *Hashemi et al* [25] for further details..

This method has the limitation of only giving average strain energy release rate (G_{Ic}) values and is, therefore, not as precise as those based on beam theory. In the case studied, the delamination is steered out of the mid-plane thereby changing the beam stiffness and applied moments via the propagating delamination front. In addition, the delamination does not propagate along the scarf in pure Mode I loading, but in a Mode I / Mode II mixity which is continuously changing as the delamination propagates away from the centre line. As this study is a comparative study of the steering mechanism, it was decided to not focus on the exact determination of the G_{Ic} using beam theory. Therefore, the much simpler area method was selected.

The external work W_{ext} was determined using a trapezoidal rule and the projection on the mid-plane of the crack length was used. For calculation the assumption was made that only one delamination propagated and the crack length was measured as a projection on the mid-plane.

2. *Tensile Testing*

Tensile tests were performed on a Schenck Hydropuls PSA ® universal testing machine, equipped with a calibrated 75 kN load cell. Testing and data analysis were performed in accordance with ASTM D3039[26]. Strain was measured by video extensometry (Imetrum). Modulus was determined using the stress and strain data between 10% and 50% of the maximum strength. Specimens were tested under displacement control at a rate of 2 mm/min.

3. Flexural Testing

A Shimadzu AGS-X universal testing machine, equipped with a calibrated 1 kN load cell was used for four point bend testing, with an upper span of 30 mm and lower span of 90 mm. Testing and data analysis were performed in accordance with ISO14125[27]. Mid-point deflection was measured via video extensometry (Imetrum).

The flexural stress σ_f [MPa], strain ϵ [mm/mm] on the outer surface and flexural modulus E_f are defined as follows:

$$\sigma_f = \frac{F \cdot L}{b \cdot h^2} \tag{2}$$

$$\epsilon = \frac{4.7 \cdot s \cdot h}{L^2} \tag{3}$$

$$E_f = \frac{0.21 \cdot L^3}{b \cdot h^3} \cdot \frac{F_{0.0025} - F_{0.0005}}{s_{0.0025} - s_{0.0005}} \tag{4}$$

Where F is the load [N], L is the outer span [mm], b is the width [mm], h is the specimen height [mm] and s is the mid-point deflection. $F_{0.0005}$ and $F_{0.0025}$ refer to the load and $s_{0.0025}$ and $s_{0.0005}$ to the mid-point deflection at a strain of 0.0005 and 0.0025 respectively.

Specimens were tested under displacement control at a rate of 5 mm/min

C. Test results and discussion

1. Micrographic analysis

Micrographs (Olympus Microscope) were taken of the polished edges of the tensile test specimens. These micrographs are shown in Fig. 1. Prior to testing, the scarf lengths and scarf angles were measured and are summarized in Table 1. The theoretical value was determined using the average measured ply thickness of 0.133 mm.

The differences between the measured and theoretical values can be explained by the fact that the specimens were manufactured by hand lay-up, where precision is limited by operator skill. However, with an automated manufactured procedure (e.g. automatic tape laying (ATL) machine), higher accuracies can be achieved.

Table 1. Summary of the scarf length and scarf angle of the tensile specimens. 6 specimens inspected. In brackets one standard deviation.

	Scarf length [mm]		Scarf Angle [°]	
	Experimental	**Theoretical**	**Experimental**	**Theoretical**
ID B	4.24 (0.32)	4	11.1 (1.0)	14.9
ID D	16.20 (0.23)	16	4.1 (0.6)	3.8

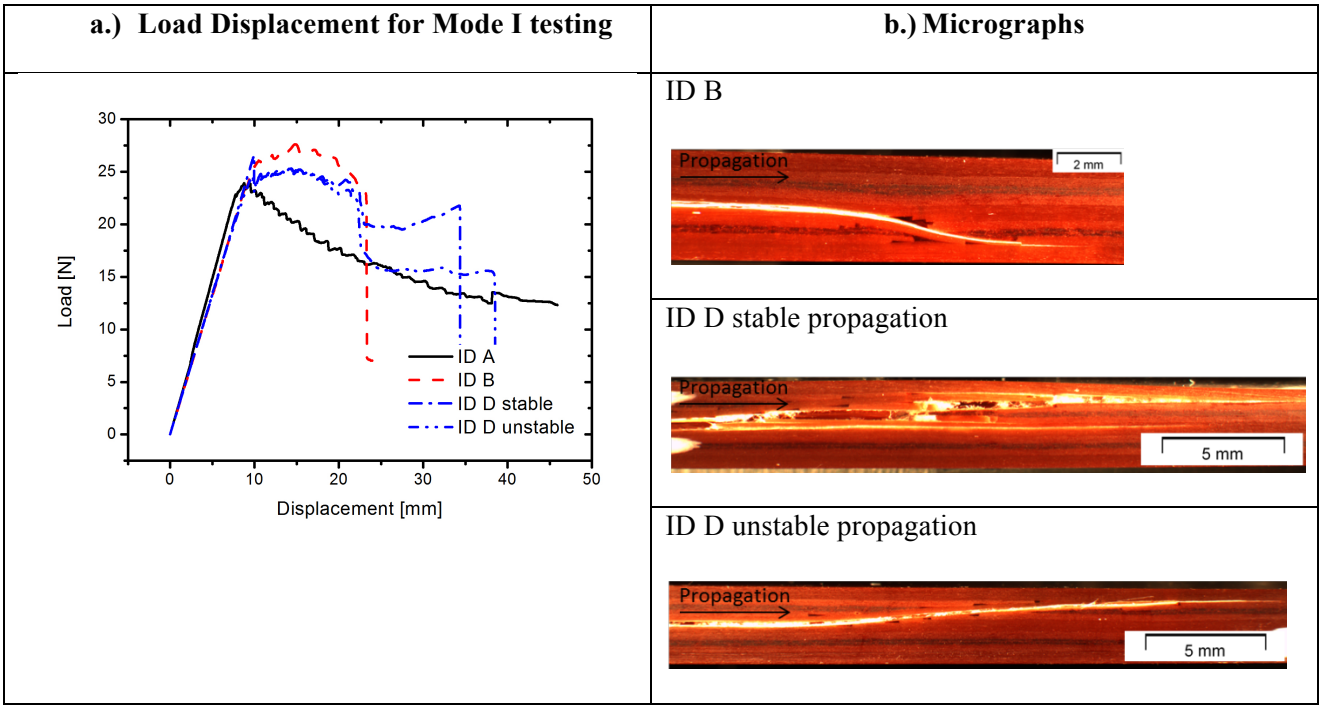

Fig. 2. a) Load-displacement results for Mode I testing, and b.) micrographs showing the delamination migration.

2. Mode I loading

Figure 2 shows the load-displacement behaviour for representative samples and the damage progression along the oblique plies. For the determination of the fracture toughness according to the area method, it was assumed that a single delamination is present in the specimen. Specimens with butt joined plies were not tested in Mode I.

The baseline specimen followed the typical load displacement plot in Mode I loading, whereas in all specimens with oblique plies, damage was steered out of the mid-plane, showing some toughening effect on the load-displacement curve.

All ID B specimens failed in an unstable manner as the propagating delamination reached the onset of the oblique layer. Thereby, the feature acted similarly to a hinge losing its load carrying capability. The delamination was observed to propagate along the oblique ply without any branching. It is assumed that the resin pocket ahead of the crack front locally increases the toughness due to the increase of resin rich interlayer thickness[28]. This ensured that the delamination followed the oblique 0° ply, which is oriented in the crack propagation direction[19,20].

In the case of the ID D specimens, 2 out of 6 showed stable delamination propagation along the complete length of the scarf. The load carrying capability was not lost and the delamination propagated in a stable manner. In these cases the delaminations branched and propagated both along the mid-plane 0°/0° interface and the oblique ply. Additional branching was observed along the oblique ply. In one case, the delamination did not propagate along the complete length of the scarf but only two plies upwards, propagating along a 0°/45° interface. In two cases, unstable delamination propagation was observed with failure similar to the case of ID B. In one case, the delamination first propagated in a stable manner, before turning unstable.

It is assumed that the difference in behaviour is due to the nature of the resin pockets along the length of the ply cuts to accommodate the oblique ply which are stochastic in nature. In terms of load carrying capability, a certain proportion remains while the delaminations are propagating along the scarfed ply interface.

It has to be noted that the sub-laminates of the DCB specimens are not symmetric and, therefore, warping of the sub-laminates occurred. In the present study, this effect has not been taken into account, as the aim of this study was simply to determine an ability to redirect delaminations through the thickness of the specimen.

Table 2. Summary of the fracture Mode I test results. 6 specimens tested per configuration. In brackets one standard deviation

	Fracture toughness G_{Ic} [J/m^2]	Percentage change	Observation
ID A	303 (28)	-	
ID B	570 (37)	+88%	
ID D all	824 (238)	+172%	
ID D stable	1121 (102)	+270%	2 specimens
ID D unstable	681(95)	+125%	2 specimens

The values of the fracture toughness are summarized in Table 2. By the introduction of the very acute scarfed ply (ID B) it is possible to increase the G_{Ic} value by 88%. For the case of the less acute configuration, a very large standard deviation for the G_{Ic} was observed giving a coefficient of variation of 29%. This is due to the fact, that as described previously, competing failure modes are present. If only the specimens with stable propagation are taken into account, the G_{Ic} is increased by a factor of 3.7. Also, in the case of unstable propagation, which is the worst case in terms of G_{Ic}, this value is increased by a factor of 1.3.

The reason for the increase in fracture toughness is due to the fact that the delaminations are moved away from their preferred propagation plane and direction. In addition, the calculated value of G_{Ic} is only an implied value, as delamination branching occurs. However, whilst observed in the majority of specimens, this this has not been taken into account in the calculations.

It can be concluded that it is possible to steer the damage progression with oblique plies and as the delamination deviates from the preferred propagation plane and direction, the Mode I fracture strain energy release rate increases.

3. Tensile tests

Figure 3 shows typical tensile test results for the different configurations tested. The local change of ply structure was found to have no significant effect on stiffness (Table 3). However, as a result of local weakening (interrupted ply structure and resin pockets) a reduction in tensile strength was observed. For the very acute (ID B) ply structure, the strength was reduced by 44%, and for the case of the less acute scarf angle (ID D), by 21%. For the butt joined plies (ID E), the strength was reduced by 57%. In all cases half of the plies are terminated due to the oblique ply or

the butt joint. However, in the case of the less acute specimens (ID D), the increased scarf length allows for better stress transfer, thereby increasing the failure load when compared to ID B and ID E.

The failure of the baseline specimen (ID A) as follows; failure of the 90° plies and transverse damage saturation, followed by transverse failure of the 45° and -45° plies with increasing damage saturation, finally catastrophic failure of the specimen by pull out at the end tabs once the strength of the fibres is exceeded.

Failure of the ID B saw transverse cracking at the resin pocket of the scarf both at the outside surface and inside (at around 140 MPa), followed by localised failure of the off-axis plies in the scarf length. The specimen then delaminates instantaneously along the scarf at maximum load. The delamination propagates until reaching the centre line where it propagates outwards along the 0°/0° interface for the complete specimen length (at maximum load carrying capability). The specimen section without a scarf retains a certain proportion of load bearing capability, as seen on the stress - displacement trace (refer to Fig. 3). Finally, a typical failure of a quasi-isotropic laminate is observed, with first failure of the off-axis plies followed by catastrophic failure of the specimen.

The failure mechanism for ID D was similar to ID B, however, due to the less acute angle, the stress transfer is better across the scarf. Therefore, the delamination initiated at this joint is at a 40% higher load than for the very acute configuration. The sub-laminate without the scarf also suffers off-axis damage, reducing the load carrying capability after delamination propagation.

For the specimen with the butt joined plies (ID E), the first damage of the resin pocket is at approximately 75 MPa. This is also observable on the stress-displacement plot (refer to Fig. 3) where a slight load decrease is visible. First, the delamination that initiates at these resin pockets propagates very slowly along the centre line. During this process, which extends for several millimetres, the load continuous to increase. The delamination then spreads more quickly to the end tabs of the specimen. This fast delamination propagation occurred at a stable load, which is similar to a pseudo-ductile stress plateau. Once the entire specimen is delaminated, the undamaged sub-laminates fail by a typical quasi-isotropic tensile failure mechanism as described for ID A. This damage mechanism is in accordance with *Wisnom et al.* [29] who studied the effect of terminated interior plies.

For the cases of the scarfed ply and the butt joined plies, the sub-laminate without a feature remains undamaged to a certain extent during delamination propagation. Therefore, once the delamination has reached the end of the

specimen, a certain proportion of load carrying capability is recovered before failure at approximately 160 MPa. This behaviour could be beneficial in the design of pseudo-ductile composite materials[30].

Table 3. Summary of the tensile test results. 6 specimens tested per configuration. In brackets one standard deviation.

	Stiffness [GPa]	Percentage change	Tensile Strength [MPa]	Percentage change
ID A	20.0 (0.8)	-	373 (27)	-
ID B	20.3 (1.4)	2%	208 (16)	-44%
ID D	20.7 (1.4)	4%	293 (11)	-21%
ID E	20.9 (0.7)	4%	162 (4)	-57%

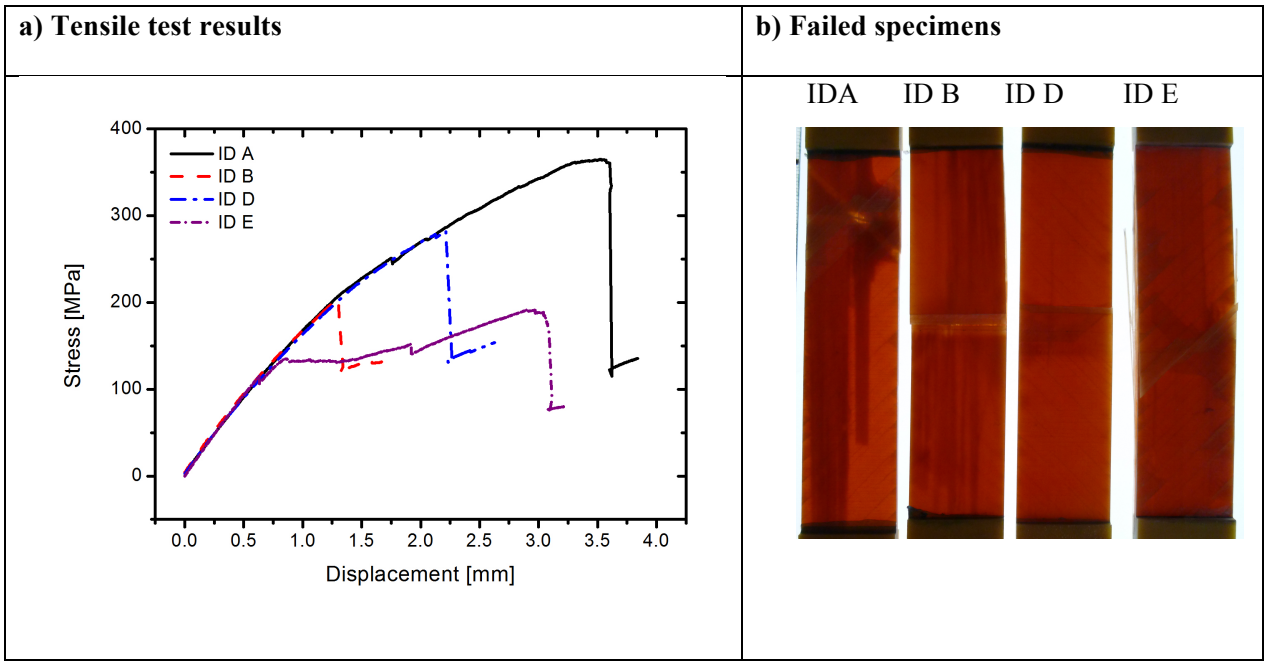

Fig. 3. a) Typical tensile test results for the different configurations, and b) through light images of failed specimens showing difference in failure mode

4. Flexural tests

Flexural tests have been performed with specimens possessing oblique plies under both tension and compression. Test results are summarized in Table 4. Figure 4 shows typical flexural test results for the different configurations. Positioning the redirection feature on the compression surface had no significant effect on flexural properties. As the

resin pockets were loaded in compression, no premature failure was observed to be initiated from these sites. In contrast, when loaded in tension, premature failure occurred due to damage initiating at the resin pocket (refer to Fig. 5) and a reduction of 10% was observed for the configuration of the acute angle (ID B) and of 24% for the butt joined plies (ID E). For configuration ID D no reduction was observed. No significant change in stiffness was observed in all cases.

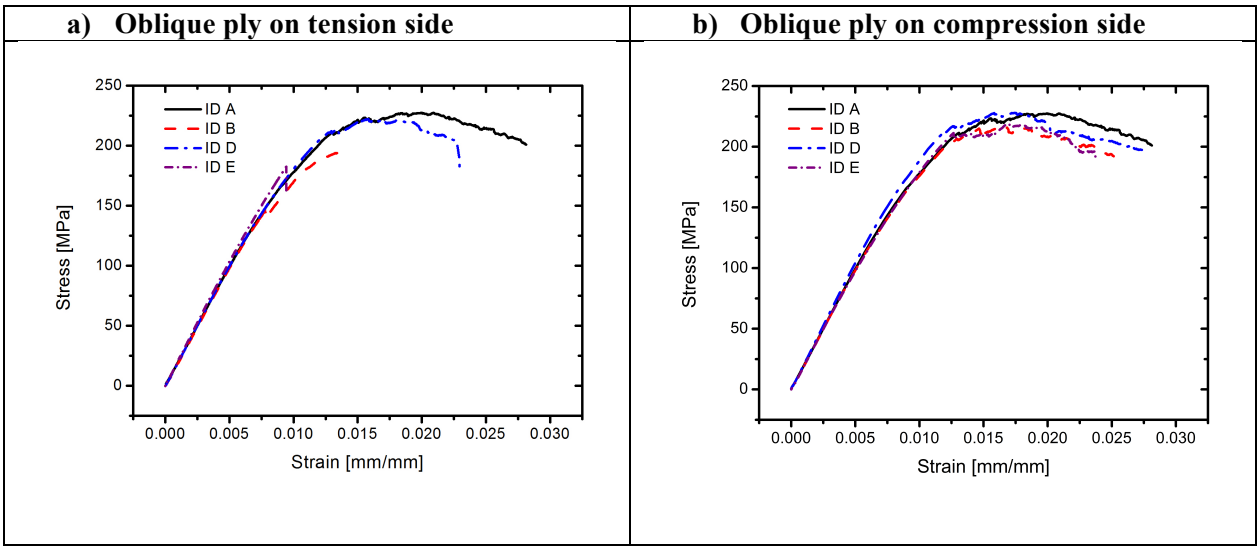

Fig. 4. Typical flexure test results a) having the oblique ply on the tension side and b) on the compression side.

Table 4 Summary of the flexure test results. 5 specimens tested per configuration. In brackets one standard deviation.

	Flexural modulus [GPa]	Percentage change	Flexural strength [MPa]	Percentage change
ID A	19.2 (0.5)	-	223 (6)	-
ID B tension side	19.9 (0.6)	4%	199 (3)	-11%
ID B compression side	19.9 (0.5)	4%	222 (6)	0%
ID D tension side	20.5 (1.1)	7%	226 (5)	1%
ID D compression side	20.1 (0.5)	5%	226 (3)	1%
ID E tension side	20.3 (1.0)	6%	170 (10)	-24%
ID E compression side	20.2 (1.1)	5%	223 (4)	0%

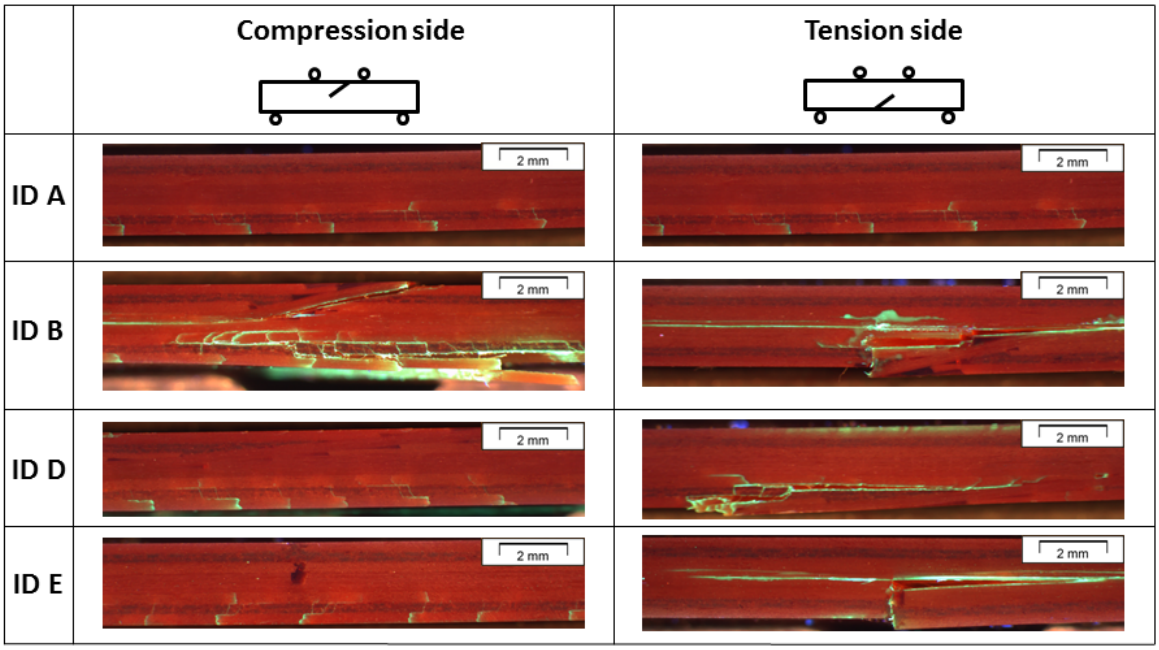

Fig. 5. Fractography of flexural samples. Damage highlighted using UV dye penetrant.

Figure 5 shows the failed specimens. The failure mode for the specimens with ID A was transverse failure of the non-zero plies located on the tension side of the sample. For the specimens of configuration B, D and E, different failure modes were present depending on the location of the oblique ply or butt joined plies. For ID B when located towards the compression side, the damage was initiated in the same way as for ID A. However, the final failure was due to a delamination initiating at the oblique ply which propagated downwards and along the central 0°/0° interface. When loaded in compression, the less acute angled specimens (ID D) exhibited the same failure mode as seen in the baseline specimens. It appears that the less steep angle ensured that the specimen did not fail at the oblique ply. When the oblique ply was towards the tension side, failure was initiated at the resin pocket of the oblique ply. For the butt joined plies (ID E), the same failure mode as for the baseline specimen, was observed when they were located towards the compression side. However, when located towards the tension side, the specimen failed along the resin pocket, before a delamination propagated along the centre line (0°/0° interface).

III. Skin-stiffener debond specimens - Feasibility study

In the following section the potential for applying this redirection mechanism to a structural feature is introduced. Skin-stiffened structures are widely used for their efficient performance in aircraft design. The reason for this is that the skin carries the in-plane loads, whereas the stiffening elements provide increased bending stiffness and a reduction in the effective buckling length. Being such a common design element, the possibility of applying the previously described delamination steering mechanism has been explored.

Testing and analysis of skin-stiffened structures is both time consuming and expensive. Therefore, *Krueger et al.*[22] developed simplified specimens, called skin-stiffener debond specimens, which mimic the stress state occurring at the tip of the flange. Due to the localised stiffening, through thickness stresses arise, which can lead to stiffener debonding. In order to overcome this problem, safety margins and inspections are scheduled, which on one hand increase the weight of the structure and on the other increase the operational costs.

One way to overcome this could be with the application of a sensor system (Structural Health Monitoring), with an autonomous repair method (self-healing) as described by *Minakuchi et al.*[31,32]. Self-healing materials[21] possess an ability to recover one or more functionalities upon a damage event. Two main approaches exist: (1) intrinsic materials, meaning that the material has the capability to restore itself upon an external stimulus and (2) extrinsic, where a healing medium is introduced via the use of microcapsules or a vascular network. The vascular approach[33–35] has several benefits over the other approaches: (1) the network can be used for other applications such as damage monitoring or thermal management. (2) The healing medium is introduced on the damage event. This means that the shelf life of the healing medium does not have to be certified beyond the design life of the host structure and that the healing medium does not react during curing of the host structure. (3) As the healing medium is introduced from an external reservoir, no restrictions on the volume exist.

One of the challenges of incorporating a vascular network into a structure is choosing its location, as the number and distribution of vascules has to remain minimal in order to reduce any detrimental effect on the host structure's performance, while ensuring the connectivity between the damage and the vascular network. One potential location for the vascular network could be the interface between the flange and the skin. In the author's opinion, this location

would be the easiest to manufacture. However, under tensile fatigue, delaminations tend to propagate downwards (refer to Fig. 7), until reaching plies oriented in the crack propagation direction[19].

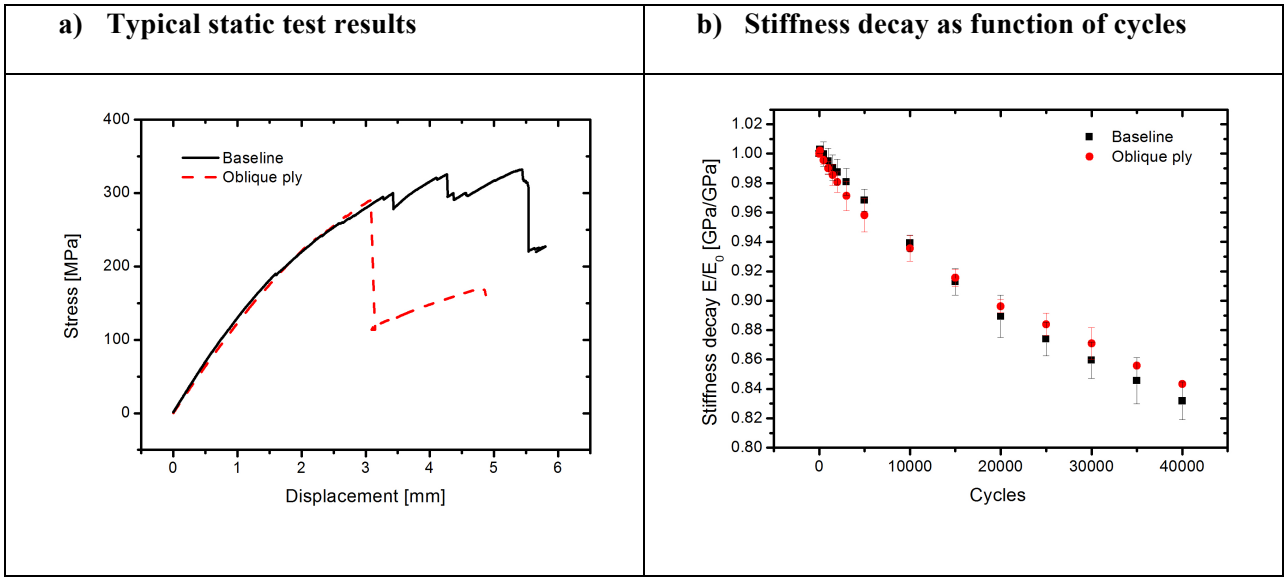

Fig. 6. a) Typical static test results and b) stiffness decay as function of cycles.

Specimens were manufactured from the same material as described above for the tensile and flexural specimens. The flange was pre-cured, cut to size (50mm length) and chamfered to 20°. The surface of the flange was then prepared for co-bonding by abrading with 500 grit SiC paper followed by cleaning with acetone. After completion, the skin and flange were assembled and cured together. The lay-up for both flange and skin was $[-45_2/90_2/45_2/0_2]_S$. For the specimen with the oblique ply, the very-acute angle configuration (ID B) was selected.

Static and fatigue tests were performed on the same testing machine as for the tensile testing described above. Static tests were performed under displacement control at a rate of 2 mm/min and fatigue tests under load control (F_{max}=10 kN, R=0.1) for 40000 cycles.

Figure 6a shows a typical stress-displacement response for static testing. It has to be noted that the ultimate tensile load (286 MPa) is reduced by approximately 15% when compared to the unmodified baseline (335 MPa). Nevertheless, the ultimate strength of the designed feature is above the first failure of the baseline configuration.

In order to assess the fatigue performance, the stiffness decay as function of cycles was monitored (Fig. 6b). Similar stiffness decay with function of cycles was observed for both configurations, but the failure mechanisms were different.

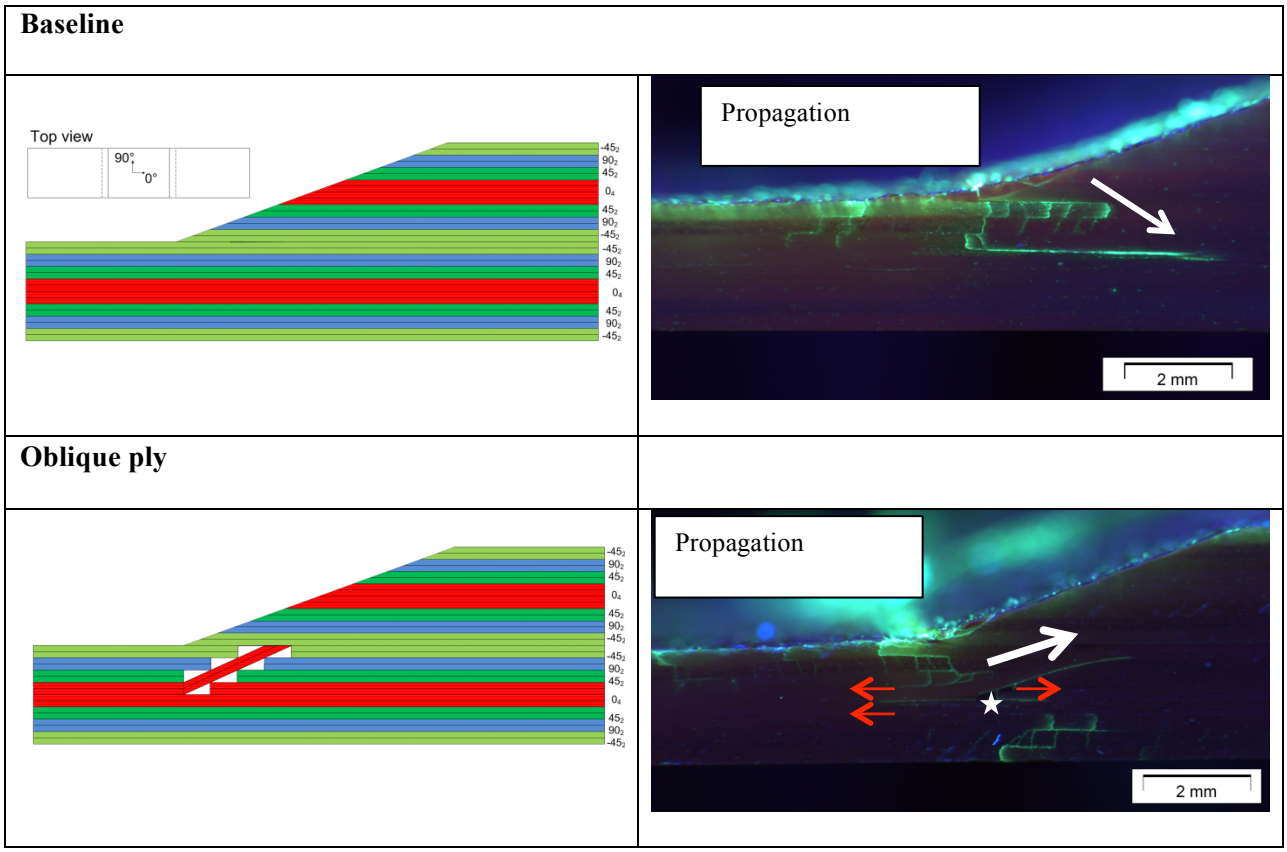

Fig. 7. Damage progression under fatigue loading. Damage highlighted with UV dye penetrant. The white arrows indicate the delamination propagation directions, red the propagation directions which could be inhibited by discrete interleaving and the star the new damage initiation locus.

For the baseline specimens, the damage initiated at the tip of the flange and then migrated inwards. Due to the resolved tensile stresses, the delamination has a tendency to migrate into lower ply interfaces. In addition, transverse damage of the off-axis plies was observed.

From the micrographs (Fig. 7) it can be observed that the delamination for the specimens with an oblique ply have a tendency to propagate into the skin-flange interface. An additional delamination initiation locus exists at the point

where the oblique plies begin (marked with a star on Fig. 7). Delaminations were seen to be initiated and propagated along the different 0° interfaces (marked with red arrows) and not only along the desired interface (marked with a white arrow). In order to promote only the selected propagation direction, other interfaces could be inhibited by locally increasing the fracture toughness as shown in the example by discrete interleaving[20].

IV. Conclusion

The ability to steer damage with oblique plies has been studied experimentally. It has been shown that a propagating delamination will follow an oblique ply when it is parallel to the crack propagation direction under static Mode I loading and under fatigue loading in a skin-stiffener debond configuration. In addition, due to the redirection of the delamination into less favourable propagation modes, the strain energy release rate increases significantly by up to 172%. This increase is explained by the fact that the delamination is moved out of its preferred propagation direction under Mode I to a Mode I / Mode II mixity which increases as the delamination is moved away from the centre line. The effect of the oblique ply structure on global properties has been studied under tension and bending.

Although no detrimental effect on stiffness was observed, the introduction of the oblique plies led to a disruption in the ply structure, significantly reducing the global tensile strength. This reduction depends on the scarf architecture, reaching 44% for the worst case. However, by reducing the scarf angle it is assumed that this detrimental effect will be reduced. In terms of flexural strength, no effect is observed when it is located towards the compression surface.

This novel ply structure could lead to a variety of innovative design solutions. Delamination arrest could be achieved by steering into a less critical region or to outside surfaces, which would additionally facilitate damage detection. The effect of delamination branching and increase in energy release rate could be used to improve crashworthiness. Finally, the delamination could be made to propagate into pre-determined areas possessing sensing and autonomous repair functionality.

Acknowledgements

This work was supported by the Engineering and Physical Sciences Research Council through the EPSRC Centre for Doctoral Training in Advanced Composites for Innovation and Science [grant number EP/G036772/1]. R. Luterbacher thanks *Fundació Obra Social la Caixa* for his scholarship.

V. References

[1] Soutis, C., "Fibre reinforced composites in aircraft construction," *Progress in Aerospace Sciences*, vol. 41, Feb. 2005, pp. 143–151.

[2] O'Brien, T. K., *Towards a damage tolerance philosophy for composite materials and structures (NASA - TM-100548)*, NASA Langley Research Center: 1988.

[3] Poe, C. C., and Kennedy, J. M., "An Assessment of Buffer Strips for Improving Damage Tolerance of Composite Laminates," *Journal of Composite Materials*, vol. 14, Jan. 1980, pp. 57–70.

[4] Yasaee, M., Killock, C., Hartley, J., and Bond, I. P., "Control of Compressive Fatigue Delamination Propagation of Impact Damaged Composites Using Discrete Thermoplastic Interleaves," *Applied Composite Materials*, vol. October, Oct. 2014.

[5] Matsuda, H., Matsubara, G., Kuraishi, A., Hirose, Y., and Hojo, M., "Effect of crack arrester on fatigue crack growth in foam core sandwich panel under mode I type loading," *Composites Part A: Applied Science and Manufacturing*, vol. 56, Sep. 2014, pp. 36–43.

[6] Dransfield, K., Baillie, C., and Mai, Y.-W., "Improving the delamination resistance of CFRP by stitching—a review," *Composites Science and Technology*, vol. 50, Jan. 1994, pp. 305–317.

[7] Yasaee, M., Bond, I. P., Trask, R. S., and Greenhalgh, E. S., "Damage control using discrete thermoplastic film inserts," *Composites Part A: Applied Science and Manufacturing*, vol. 43, Jun. 2012, pp. 978–989.

[8] Rinker, M., Zahlen, P. C., John, M., and Schauble, R., "Investigation of sandwich crack stop elements under fatigue loading," *Journal of Sandwich Structures and Materials*, vol. 14, Dec. 2011, pp. 55–73.

[9] Mouritz, A. P., "Review of z-pinned composite laminates," *Composites Part A: Applied Science and Manufacturing*, vol. 38, Dec. 2007, pp. 2383–2397.

[10] Chen, X., Ren, H., Bil, C., and Cai, J., "Repair Tolerance Analysis for Composite Structures Using Probabilistic Methodologies," *Journal of Aircraft*, vol. 51, 2014.

[11] Greenhalgh, E., and Hiley, M., "The assessment of novel materials and processes for the impact tolerant design of stiffened composite aerospace structures," *Composites Part A: Applied Science and Manufacturing*, vol. 34, Feb. 2003, pp. 151–161.

[12] Chen, X., Ren, H., and Bil, C., "Inspection Intervals Optimization for Aircraft Composite Structures Considering Dent Damage," *Journal of Aircraft*, vol. 51, 2014, pp. 303–309.

[13] Feraboli, P., and Kawakami, H., "Damage of Carbon/Epoxy Composite Plates Subjected to Mechanical Impact and Simulated Lightning," *Journal of Aircraft*, vol. 47, 2010, pp. 999–1012.

[14] Dan-Jumbo, E. A., Keller, R. L., and Westerman, E., "Composite structures employing quasi-isotropic laminates," WO 2010/104741A1, 2010.incomplete reference?

[15] Burns, L. A., Mouritz, A. P., Pook, D., and Feih, S., "Bio-inspired design of aerospace composite joints for improved damage tolerance," *Composite Structures*, vol. 94, Feb. 2012, pp. 995–1004.

[16] Kasapi, M. A., and Gosline, J. M., "Design complexity and fracture control in the equine hoof wall.," *The Journal of experimental biology*, vol. 200, Jun. 1997, pp. 1639–1659.

[17] Wang, Q., Nemoto, M., Li, D., Weaver, J. C., Weden, B., Stegemeier, J., Bozhilov, K. N., Wood, L. R., Milliron, G. W., Kim, C. S., Dimasi, E., and Kisailus, D., "Phase Transformations and Structural

Developments in the Radular Teeth of Cryptochiton Stelleri," *Advanced Functional Materials*, vol. 23, 2013, pp. 2908–2917.

[18] Wisnom, M. R., "The role of delamination in failure of fibre-reinforced composites," *Philosophical transactions. Series A, Mathematical, physical, and engineering sciences*, vol. 370, Apr. 2012, pp. 1850–1870.

[19] Singh, S., and Greenhalgh, E. S., "Micromechanics of interlaminar fracture in carbon fibre reinforced plastics at multidirectional ply interfaces under static and cyclic loading," *Plastics, rubber and composites processing and applications*, vol. 27, 1998, pp. 220–226.

[20] Purslow, D., "Some fundamental aspects of composites fractography," *Composites*, vol. 12, 1981, pp. 241–247.

[21] Blaiszik, B. J., Kramer, S. L. B., Olugebefola, S. C., Moore, J. S., Sottos, N. R., and White, S. R., "Self-Healing Polymers and Composites," *Annual Review of Materials Research*, vol. 40, Jun. 2010, pp. 179–211.

[22] Krueger, R., Cvitkovich, M. K., and O'Brien, T. K., *Testing and analysis of Composite Skin / Stringer Debonding Under multi-axial loading (NASA TM-1999-209097)*, NASA Langley Research Center: 1999.

[23] Imperiale, V. A., and Bond, I. P., "Autonomous self-healing of damaged CFRP's," *53rd AIAA/ASME/ASCE/AHS/ASC Structures, Structural Dynamics and Materials Conference*, Honolulu (Hawaii): 2012, pp. 1–9.

[24] ASTM International, "ASTM D5528-1 Standard Test Method for Mode I Interlaminar Fracture Toughness of Unidirectional Fiber-Reinforced Polymer Matrix Composites," 2012, pp. 1–12.

[25] Hashemi, S., Kinloch, A. ., and Williams, J. G., "The analysis of interlaminar fracture in uniaxial fibre-polymer composites," *Proc. R. Soc. Lond. A*, vol. 427, 1990, pp. 179–199.

[26] ASTM International, "ASTM D3039 /D3039M-08 Standard Test Method for Tensile Properties of Polymer Matrix Composite Materials," 2008, pp. 1–13.

[27] International Organization for Standardization, "EN-ISO 14125 Fibre-reinforced plastic composites," 1998.

[28] Sela, N., Ishai, O., and Banks-Sills, L., "The effect of adhesive thickness on interlaminar fracture toughness of interleaved CFRP specimens," *Composites*, vol. 20, May 1989, pp. 257–264.

[29] Cui, W., Wisnom, M. R., and Jones, M., "An Experimental and Analytical Study of Delamination of Unidirectional Specimens with Cut Central Plies," *Journal of Reinforced Plastics and Composites*, vol. 13, Aug. 1994, pp. 722–739.

[30] Czél, G., and Wisnom, M. R., "Demonstration of pseudo-ductility in high performance glass/epoxy composites by hybridisation with thin-ply carbon prepreg," *Composites Part A: Applied Science and Manufacturing*, vol. 52, Sep. 2013, pp. 23–30.

[31] Minakuchi, S., Sun, D., and Takeda, N., "Hierarchical system for autonomous sensing-healing of delamination in large-scale composite structures," *Smart Materials and Structures*, vol. 23, Oct. 2014, p. 10.

[32] Minakuchi, S., Banshoya, H., Ii, S., and Takeda, N., "Hierarchical fiber-optic delamination detection system for carbon fiber reinforced plastic structures," *Smart Materials and Structures*, vol. 21, Oct. 2012, p. 13.

[33] Trask, R. S., and Bond, I. P., "Biomimetic self-healing of advanced composite structures using hollow glass fibres," *Smart Materials and Structures*, vol. 15, Jun. 2006, pp. 704–710.

[34] Trask, R. S., Norris, C. J., and Bond, I. P., "Stimuli-triggered self-healing functionality in advanced fibre-reinforced composites," *Journal of Intelligent Material Systems and Structures*, vol. 25, Sep. 2014, pp. 87–97.

[35] Coope, T. S., Wass, D. F., Trask, R. S., and Bond, I. P. I. P., "Metal Triflates as Catalytic Curing Agents in Self-Healing Fibre Reinforced Polymer Composite Materials," *Macromolecular Materials and Engineering*, vol. 299, Feb. 2014, pp. 208–218.

[36] Yasaee, M., Bond, I. P., Trask, R. S., and Greenhalgh, E. S., "Mode I interfacial toughening through discontinuous interleaves for damage suppression and control," *Composites Part A: Applied Science and Manufacturing*, vol. 43, 2012, pp. 198–207.